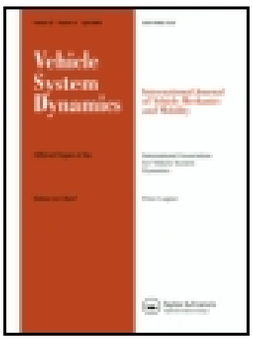

Vehicle System Dynamics

ISSN: 0042-3114 (Print) 1744-5159 (Online) Journal homepage: http://www.tandfonline.com/loi/nvsd20

Analyses of Vision-based Lateral Control for Automated Highway System

JIN-CHUAN HSU Visiting graduate student & MASAYOSHI TOMIZUKA Professor

To cite this article: JIN-CHUAN HSU Visiting graduate student & MASAYOSHI TOMIZUKA Professor (1998) Analyses of Vision-based Lateral Control for Automated Highway System, Vehicle System Dynamics, 30:5, 345-373, DOI: 10.1080/00423119808969456

To link to this article: http://dx.doi.org/10.1080/00423119808969456

Vehicle System Dynamics, 30 (1998), pp. 345–373 0042-3114/98/3005-345$12.00

Analyses of Vision-based Lateral Control for Automated Highway System

JIN-CHUAN HSU[†] and MASAYOSHI TOMIZUKA[‡]

SUMMARY

The stability and performance of a vision-based vehicle lateral control system are analyzed. Effects of look-ahead distance, vision delay, and vehicle speed on the performance of vision feedback control system are examined by using frequency domain and time domain methods. A measurement model of the vision system is derived from the point of view of multiple sensors. The quantization error of the vision system is analyzed and the way of extracting essential information for control is studied. Based on this analysis, some guidelines for the design of vision-based controllers are proposed. A design example is further illustrated for a vision system with a substantial time delay.

1. INTRODUCTION

Vision-based lateral control of vehicles is expected to play a key role in developing automated highway systems (AHS). The vision system can provide information on the road ahead of the vehicle as well as on the vehicle's motion relative to the road, which makes the lateral control possible without any special reference system on the road. When reference systems such as the ones based on magnetic nails are installed on automated lanes, the vision system is still useful for lane-change maneuvers. The objective of this study is to analyze the effect of parameters in the vision system on the stability and performance of the lane-following controller based on vision. Key parameters are: (a) look ahead distance (b) vehicle speed and (c) delay time in the vision system.

Research on vision-guidance for applications to automatic guided vehicles and advanced road vehicles has been conducted for some years. An excellent survey on the vision-based vehicle guidance has been presented in [1]. Previous studies

[†] Visiting graduate student, Department of Mechanical Engineering, University of California, Berkeley. Department of Power Mechanical Engineering, National Tsing Hua University, HsinChu, Taiwan 30043, R.O.C.

[‡] Professor. Author for correspondence. Department of Mechanical Engineering, University of California, Berkeley, CA 94720, U.S.A.

have mostly focused on the development of real-time image processing algorithms for lane finding, road geometry identification, obstacle detection and traffic sign recognition.

For the purpose of vehicle lateral control for lane following, Dickmanns et al. [2,3] proposed a vision-based estimation scheme to obtain the curvature and vehicular state variables. By utilizing the road-vehicle kinematics and a curvature generation model, those variables are recursively estimated by a Kalman filter. The future curvature and the vehicle state variables are essential to realize the lateral control systems proposed to date. For examples, Peng et al. [4] and Lee [5] proposed continuous time and discrete time preview control schemes, respectively, for the lateral guidance of the vehicle. The lateral controller with preview has been analyzed to understand the performance improvement by preview [4]. However, the basic properties of the lateral control system with vision, such as stability and performance limitations, have not been fully studied.

Recently, a fundamental analysis of the automatic steering control with look-down lateral references has been conducted by Guldner et al. [6]. The performance and stability of the system were investigated using the frequency response and root locus techniques. Effects of the longitudinal velocity, the road friction coefficient, and the distance between the vehicle's center of gravity (c.g.) and the lateral displacement sensor were examined. These results are relevant to systems with look-ahead sensors such as vision sensors. However, some distinct characteristics of the vision system such as projection geometry, image discretization, vision delay, and preview of the road require further design considerations of the steering control system with vision. In this paper, these characteristics are studied from the viewpoint of AHS applications. Some guidelines for the control design to properly deal with the road curvature disturbances and the vision delay are proposed. Finally, a design example is given.

NOMENCLATURE

Y_e	Lateral deviation of vehicle's c.g.
φ_h	Heading angle of the vehicle (yaw angle relative to the road direction)
r	Yaw rate
β	Sideslip angle of the vehicle body
ℓ	Look ahead distance
n	Sensor noise
y	Measured lateral error in the image plane (vision output)
Y	Lateral error in road plane corresponding to the vision output
C_f, C_r	Cornering stiffness of front and rear tires
a, b	Distance from front and rear axles to c.g.
c	Pixel length
δ	Tire steer angle

f Focal length of camera
m Vehicle mass
I_z Moment inertia about c.g. for yaw motion
U Longitudinal velocity of the vehicle
ρ Road curvature
W_{im} Width of the image plane
S Road curvilinear coordinate
$X - Y$ Vehicle-fixed coordinate

2. VEHICLE DYNAMICS MODEL

The vehicle lateral dynamics can be represented by a two degrees of freedom (2 d.o.f.) bicycle model:

$$\frac{\mathrm{d}\boldsymbol{x}}{\mathrm{d}t} = \begin{bmatrix} \dot{r} \\ \dot{\beta} \\ \dot{\varphi}_h \\ \dot{Y}_e \end{bmatrix} = \begin{bmatrix} \dfrac{-2(a^2C_f + b^2C_r)}{I_z U} & \dfrac{-2aC_f + 2bC_r}{I_z} & 0 & 0 \\ \dfrac{-2aC_f + 2bC_r - mU^2}{mU^2} & \dfrac{-2(C_f + C_r)}{mU} & 0 & 0 \\ 1 & 0 & 0 & 0 \\ 0 & U & U & 0 \end{bmatrix} \begin{bmatrix} r \\ \beta \\ \varphi_h \\ Y_e \end{bmatrix}$$

$$+ \begin{bmatrix} \dfrac{2aC_f}{I_z} & 0 \\ \dfrac{2C_f}{mU} & 0 \\ 0 & -U \\ 0 & 0 \end{bmatrix} \begin{bmatrix} \delta \\ \rho \end{bmatrix} = \mathbf{A}\boldsymbol{x} + [\mathbf{B}_1 \quad \mathbf{B}_2] \begin{bmatrix} \delta \\ \rho \end{bmatrix} \tag{1}$$

where $\boldsymbol{x} = [r \quad \beta \quad \varphi_h \quad Y_e]^T$ is the vector of vehicle state variables; r is the yaw rate, β is the sideslip angle of the vehicle body, φ_h is the heading angle defined as the relative yaw angle between the vehicle heading direction and the road tangential direction, Y_e is the lateral deviation at the vehicle's c.g., δ is the tire steer angle, and ρ is the road curvature. Other symbols are defined in the Nomenclature. This model is applicable to the cases with low lateral accelerations (smaller than 0.3 g) and stiff suspensions [7].

Figure 1 shows the vehicle-road relationship and the lateral offset Y at a certain look-ahead distance ℓ and at time t along with the corresponding view in the image plane. The vehicle-fixed coordinate is defined to make this measurement

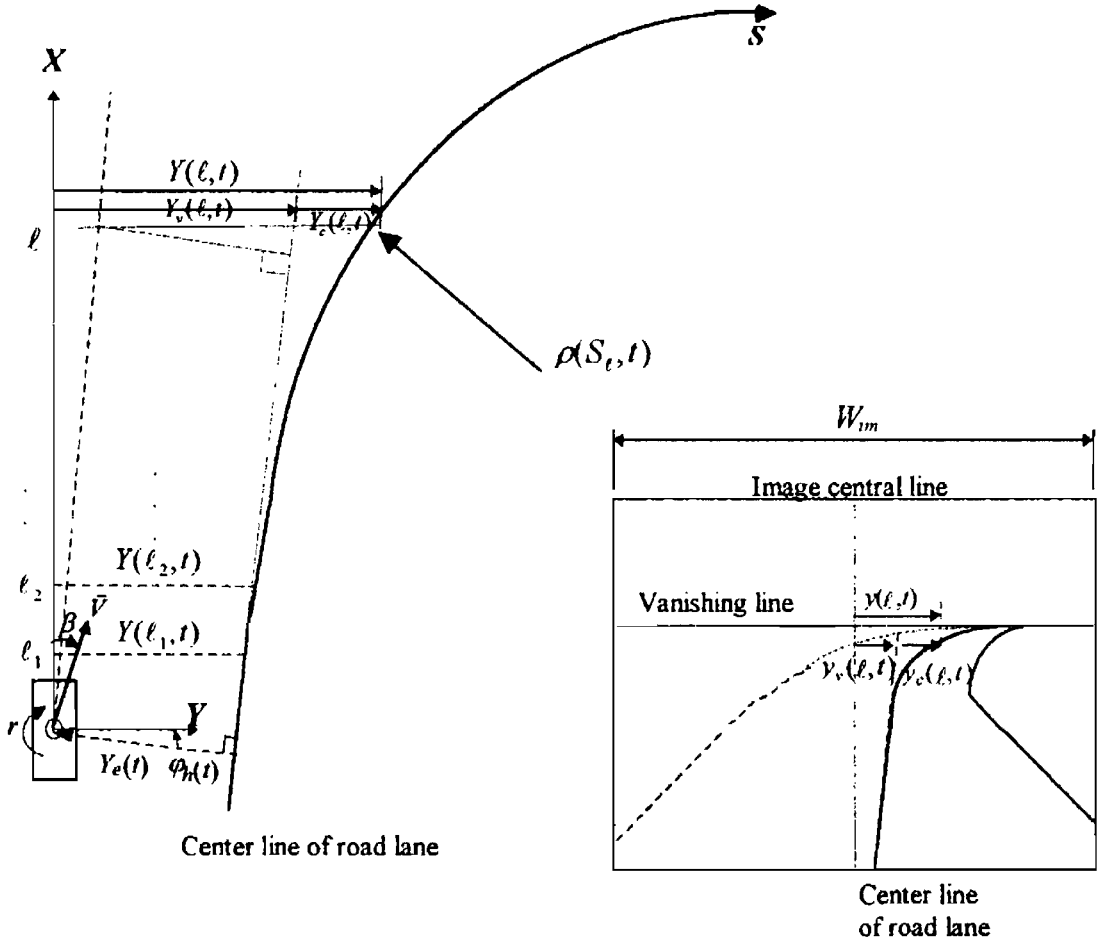

Fig. 1. Road-vehicle geometric relationship and corresponding view in image plane.

available by the in-vehicle vision sensor. Under some road geometry and vehicle motion assumptions, which are reasonable for the AHS application, the lateral offset represented on the road plane can be derived as

$$Y(\ell, t) = \left(-Y_e(t) - \ell \sin \varphi_h(t) + \int_0^{S_\ell} \int_0^{S_\ell} \rho(S, t)\, dS\, dS \right) \frac{1}{\cos \varphi_h(t)}$$

$$\approx -Y_e(t) - \ell \varphi_h(t) + \int_0^{\ell} \int_0^{\ell} \rho(X, t)\, dX\, dX$$

(if the road curvature is mild and $\varphi_h(t)$ is small)

$$\approx -Y_e(t) - \ell \varphi_h(t) + \frac{\ell^2}{2} \rho\left(\frac{\ell}{2}, t\right)$$

(if the change of curvature is linear and slow)

$$\approx -Y_e(t) - \ell\varphi_h(t) + \frac{\ell^2}{2}\rho\left(t + \frac{\ell}{2U}\right)$$

(if the vehicle is almost following the road)

$$= Y_v(\ell, t) + Y_c(\ell, t) \tag{2}$$

where $Y_v(\ell, t) = -Y_e(t) - \ell\varphi_h(t)$ and $Y_c(\ell, t) = \frac{\ell^2}{2}\rho\left(t + \frac{\ell}{2U}\right)$. Note that the lateral offset Y consists of two components: Y_v due to the vehicle's angle and position relative to the road and Y_c due to the road curvature.

3. VISION SYSTEM

3.1. Prospective Geometry

According to the prospective geometry of the camera as shown in Figure 2, the point projection from the road plane to the image plane can be described by

$$v(\ell, t) = \frac{f}{\ell} Y(\ell, t), \tag{3}$$

where f is the focal length of the camera. Y represents the lateral location of a road-center marker **P** with a look-ahead distance ℓ on the road plane. This location is expressed in the vehicle-fixed coordinate $X - Y$. y is the lateral location of the point **P** projected in the image plane in terms of the image-plane-fixed coordinate $x - y$. The image plane is set perpendicular to the road plane, and the y-axis in the image plane is arranged to be parallel to the Y-axis in the road plane. It also represents the scanning level related to the infinite look-ahead

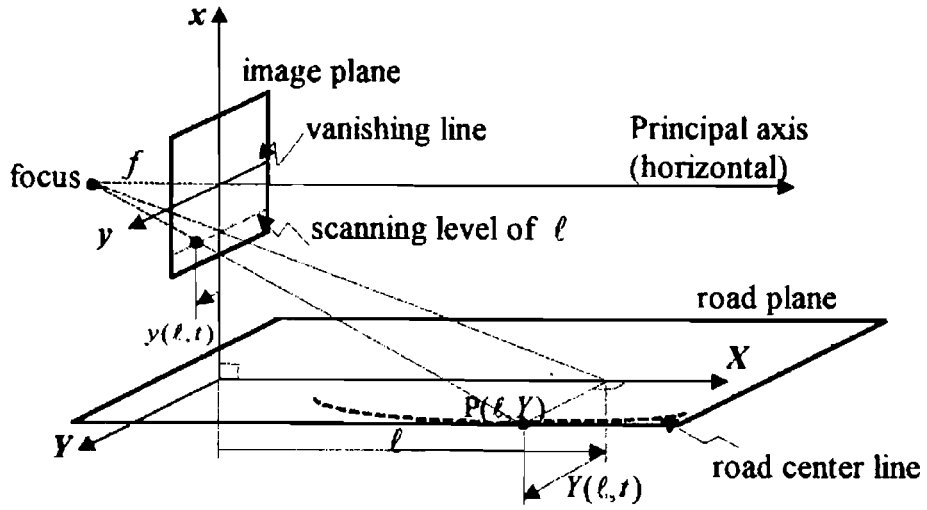

Fig. 2. Perspective geometry of the image plane relative to the road plane.

distance at which the size of every object diminishes to a point in the image plane. Thus, it is called the vanishing line by this property of prospective geometry. The lower the scanning level, the closer the scanned area to the vehicle's c.g.

3.2. Resolution due to Image Quantization

The grabbed picture by the CCD camera is actually a discretized image with finite pixels. The measurement accuracy is limited by the image resolution, and the effect of quantization errors on the control system performance is a concern of the designer.

Let Y_m and y_m be the measured values of lateral offsets on the real road plane and the image plane respectively. These measurements are taken at a look ahead distance ℓ. Then the error range due to the image quantization is

$$| Y - Y_m | = \frac{\ell}{f} | y - y_m | = \frac{c\ell}{f} \left| \frac{y}{c} - \left[\frac{y}{c} \right] \right| \leq \frac{c\ell}{2f}, \tag{4}$$

where $[\cdot]$ is the closest integer to $\cdot$, c is the interval length of a pixel, Y and y represent the actual values of lateral offsets. This inequality implies that the variation of lateral offset smaller than $\frac{c\ell}{2f}$ can not be resolved. Notice that the quantization error may be reduced by decreasing the look-ahead distance ℓ or by decreasing c, i.e., using a camera with a higher resolution. On the other hand, the focal length f may be increased to reduce this error, but it will make the

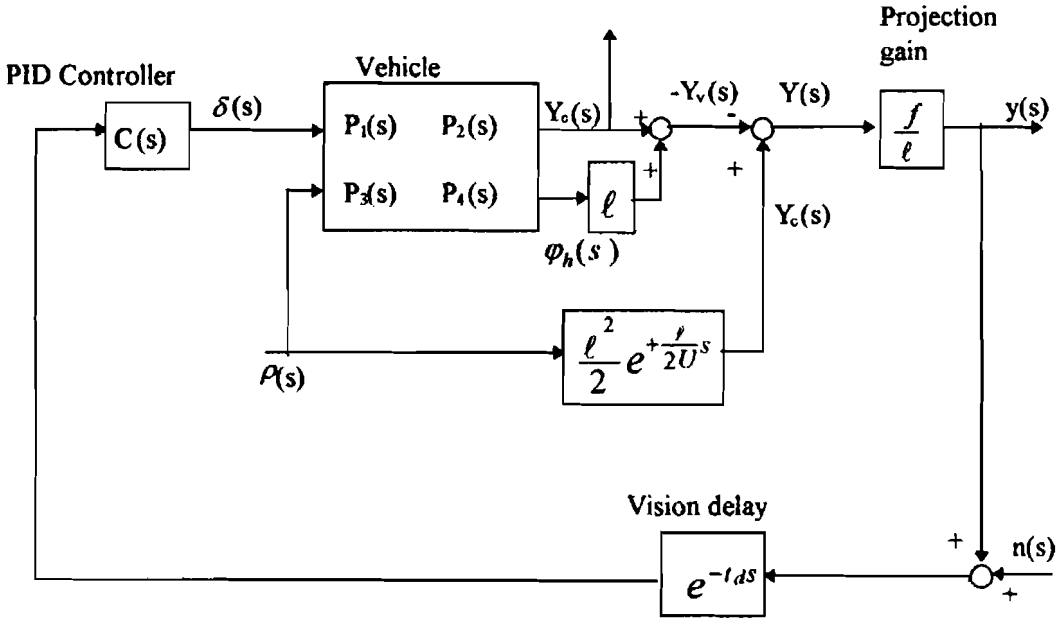

Fig. 3. Block diagram of the basic lateral control system with vision.

measurement range smaller. The visual angle θ, which represents the measurement range, is

$$\theta = \frac{W_{im}}{f}$$

where W_{im} is the width of the image plane. Since W_{im} is fixed, the extension of the focal length f will decrease the visual angle.

3.3. Measurement Matrix

According to Equations (2) and (3), the measured lateral offset on the image plane, i.e., the vision output, y, can be expressed as

$$y(\ell, t) = \frac{f}{\ell}\left(-Y_e(t) - \ell \sin \varphi_h(t) + \frac{\ell^2}{2}\rho\left(t + \frac{\ell}{2U}\right)\right)$$

$$= \left[0 \quad 0 \quad -f \quad -\frac{f}{\ell}\right] X(t) + \frac{f\ell}{2}\rho\left(t + \frac{\ell}{2U}\right)$$

$$= H(\ell)\, X(t) + \frac{f\ell}{2}\rho\left(t + \frac{\ell}{2U}\right)$$

$$= H_1(\ell)\begin{bmatrix}\varphi_h(t) \\ Y_e(t)\end{bmatrix} + \frac{f\ell}{2}\rho\left(t + \frac{\ell}{2U}\right)$$

$$= y_v(\ell, t) + y_c(\ell, t) \tag{5}$$

where

$$H(\ell) = \left[0 \quad 0 \quad -f \quad -\frac{f}{\ell}\right], \; H_1(\ell) = \left[-f \quad -\frac{f}{\ell}\right],$$

$$y_v(\ell, t) = -f\varphi_h(t) - \frac{f}{\ell}Y_e(t),$$

and

$$y_c(\ell, t) = \frac{f\ell}{2}\rho\left(t + \frac{\ell}{2U}\right).$$

For straight roads, the curvature is zero and we obtain

$$\lim_{\ell \to \infty} y(\ell, t) = -f\varphi_h(t) \tag{6}$$

This means that the location of vanishing point represents the vehicle heading direction. From Equation (5), it is observed that the contribution of the lateral deviation to the vision output is more pronounced as the look ahead distance gets shorter. On the other hand, the component due to curvature in the vision output is augmented by increasing the look ahead distance.

The camera can grab the image ranging from a certain distance in front of c.g. to the infinite look-ahead distance. All scanning levels of the image plane below the vanishing line can be used as measurements: i.e., the vision output is equivalent to multiple sensors. Therefore,

$$\mathbf{y}(t) = \begin{bmatrix} y(\ell_1, t) \\ y(\ell_2, t) \\ \vdots \\ y(\ell_N, t) \end{bmatrix}$$

$$= \begin{bmatrix} 0 & 0 & -f & -\dfrac{f}{\ell_1} \\ 0 & 0 & -f & -\dfrac{f}{\ell_2} \\ \vdots & \vdots & \vdots & \vdots \\ 0 & 0 & -f & -\dfrac{f}{\ell_N} \end{bmatrix} \mathbf{X}(t) + \begin{bmatrix} \dfrac{f\ell_1}{2}\rho\left(t + \dfrac{\ell_1}{2U}\right) \\ \dfrac{f\ell_2}{2}\rho\left(t + \dfrac{\ell_2}{2U}\right) \\ \vdots \\ \dfrac{f\ell_N}{2}\rho\left(t + \dfrac{\ell_N}{2U}\right) \end{bmatrix}$$

$$= \mathbf{H}\mathbf{X}(t) + \mathbf{F}\left(\rho\left(t + \frac{\ell_1}{2U}\right), \ldots, \rho\left(t + \frac{\ell_N}{2U}\right)\right)$$

$$= \mathbf{H}_1 \begin{bmatrix} \varphi_h(t) \\ Y_e(t) \end{bmatrix} + \mathbf{F}\left(\rho\left(t + \frac{\ell_1}{2U}\right), \ldots, \rho\left(t + \frac{\ell_N}{2U}\right)\right)$$

$$= \mathbf{y}_v(t) + \mathbf{y}_c(t) \tag{7}$$

where N is the number of scanning levels, and

$$\mathbf{H} = \begin{bmatrix} 0 & 0 & -f & -\dfrac{f}{\ell_1} \\ 0 & 0 & -f & -\dfrac{f}{\ell_2} \\ \vdots & \vdots & \vdots & \vdots \\ 0 & 0 & -f & -\dfrac{f}{\ell_N} \end{bmatrix}; \quad \mathbf{H}_1 = \begin{bmatrix} -f & -\dfrac{f}{\ell_1} \\ -f & -\dfrac{f}{\ell_2} \\ \vdots & \vdots \\ -f & -\dfrac{f}{\ell_N} \end{bmatrix}; \quad \mathbf{y}_v(t) = \begin{bmatrix} y_v(\ell_1, t) \\ y_v(\ell_2, t) \\ \vdots \\ y_v(\ell_N, t) \end{bmatrix}$$

$$\mathbf{y}_c(t) = \begin{bmatrix} y_c(\ell_1, t) \\ y_c(\ell_2, t) \\ \vdots \\ y_c(\ell_N, t) \end{bmatrix}; \quad \mathbf{F}\left(\rho\left(t + \frac{\ell_1}{2U}\right), \ldots, \rho\left(t + \frac{\ell_N}{2U}\right)\right) = \begin{bmatrix} \dfrac{f\ell_1}{2}\rho\left(t + \dfrac{\ell_1}{2U}\right) \\ \dfrac{f\ell_2}{2}\rho\left(t + \dfrac{\ell_2}{2U}\right) \\ \vdots \\ \dfrac{f\ell_N}{2}\rho\left(t + \dfrac{\ell_N}{2U}\right) \end{bmatrix}$$

The measurement matrix $\mathbf{y}(t)$ can be used to extract the essential state variables of the vehicle and the road curvatures ahead of the vehicle.

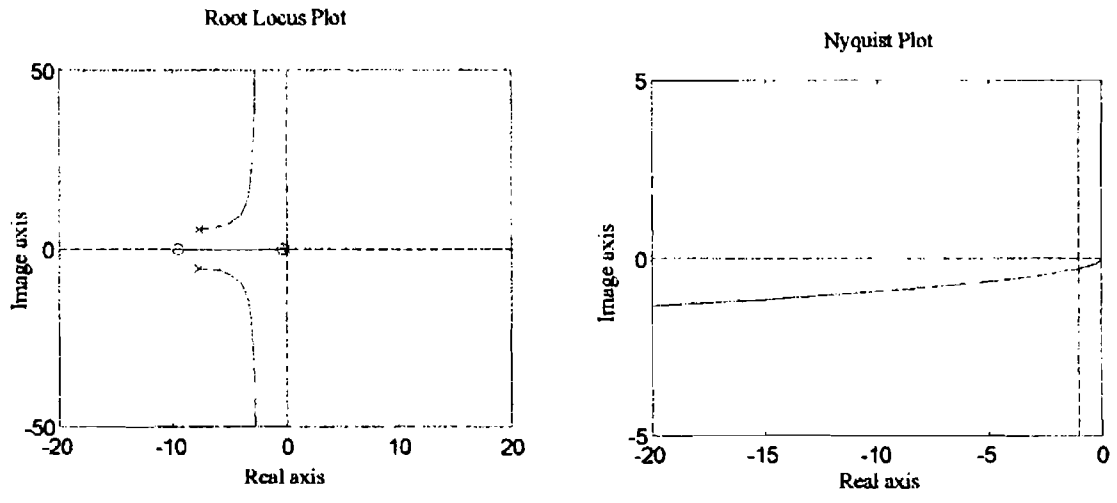

Fig. 4. Stability analysis for $\ell = 100$ m, $U = 30$ m/s, and $t_d = 0$ s. (stable) (a) Root locus (b) Nyquist plot, for unity feedback.

4. DIRECT VISION-OUTPUT FEEDBACK CONTROL SYSTEM

4.1. System Configuration

To investigate some fundamental characteristics of the vision-based lateral control system, a basic PID control system with direct feedback of the vision output is considered. The block diagram for this basic control system is shown in Figure 3. The control objective is to regulate the lateral deviation at c.g. (Y_e) to zero. The steering action is generated by the PID controller $C(s)$ with the vision output y as the feedback signal. The feedback includes a time delays caused by the sampling and processing of the image. The road curvature enters the system as a disturbance to cause the vehicle to deviate from the center line of the road. The PID controller is used to attenuate this effect. In practical cases, there is a sensor noise n added to the vision-output which deteriorates the system performance.

The vehicle transfer function in Figure 3 is obtained from Equation (1) and is written as

$$\begin{bmatrix} Y_e(s) \\ \varphi_h(s) \end{bmatrix} = \begin{bmatrix} P_1(s) & P_2(s) \\ P_3(s) & P_4(s) \end{bmatrix} \begin{bmatrix} \delta(s) \\ \rho(s) \end{bmatrix} \tag{8}$$

where

$$\begin{aligned} P_1(s) &= [0 \quad 0 \quad 0 \quad 1](s\mathbf{I} - \mathbf{A})^{-1}\mathbf{B}_1 = \mathbf{h}_1(s\mathbf{I} - \mathbf{A})^{-1}\mathbf{B}_1 \\ P_2(s) &= [0 \quad 0 \quad 0 \quad 1](s\mathbf{I} - \mathbf{A})^{-1}\mathbf{B}_2 = \mathbf{h}_1(s\mathbf{I} - \mathbf{A})^{-1}\mathbf{B}_2 \\ P_3(s) &= [0 \quad 0 \quad 1 \quad 0](s\mathbf{I} - \mathbf{A})^{-1}\mathbf{B}_1 = \mathbf{h}_2(s\mathbf{I} - \mathbf{A})^{-1}\mathbf{B}_1 \\ P_4(s) &= [0 \quad 0 \quad 1 \quad 0](s\mathbf{I} - \mathbf{A})^{-1}\mathbf{B}_2 = \mathbf{h}_2(s\mathbf{I} - \mathbf{A})^{-1}\mathbf{B}_2 \end{aligned} \tag{9}$$

$$\mathbf{h}_1 = [0 \quad 0 \quad 0 \quad 1] \text{ and } \mathbf{h}_2 = [0 \quad 0 \quad 1 \quad 0].$$

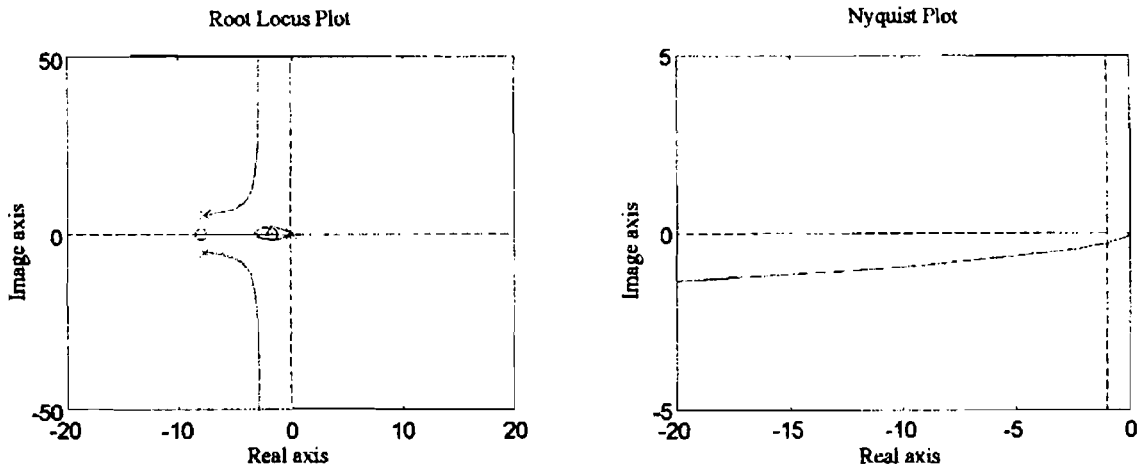

Fig. 5. Stability analysis for $\ell = 20$m, $U = 30$m/s, and $t_d = 0$ s. (stable) (a) Root locus (b) Nyquist plot, for unity feedback.

The PID controller is expressed as

$$C(s) = K_p + \frac{K_d s}{T_i s + 1} + \frac{K_i}{s} \tag{10}$$

In the following analysis, a unity feedback controller, i.e., $C(s) = K_p = 1$, is used in most parts to simplify the analysis. Referring to Figure 3, the steer angle generated by the unity feedback controller can be written as

$$\begin{aligned} \delta(s) &= y(s) e^{-t_d s} \\ &= \frac{f}{\ell} Y_v(s) e^{-t_d s} + \frac{f}{\ell} Y_c(s) e^{-t_d s} \end{aligned} \tag{11}$$

The first term in the right-hand side of Equation (11) represents the feedback action caused by the motion error, $Y_v(\ell, t) = -Y_e(t) - \ell \varphi_h(t)$. The second term represents the feedforward action due to the previewed road curvature, $Y_c(\ell, t) = \frac{\ell^2}{2} \rho\left(t + \frac{\ell}{2U}\right)$.

4.2. Stability Analysis

To obtain a rough physical sense about the closed-loop stability, we consider the simplest unity feedback case without vision delay. From Equations (1) and (5), the vision output can be written as

$$\begin{aligned} y(\ell, t) &= -f\varphi_h(t) - \frac{f}{\ell} Y_e(t) + \frac{f\ell}{2} \rho\left(t + \frac{\ell}{2U}\right) \\ &\approx \frac{-f}{U} \dot{Y}_e(t) - \frac{f}{\ell} Y_e(t) + \frac{f\ell}{2} \rho\left(t + \frac{\ell}{2U}\right) \quad \text{(if } \beta \text{ small)} \end{aligned} \tag{12}$$

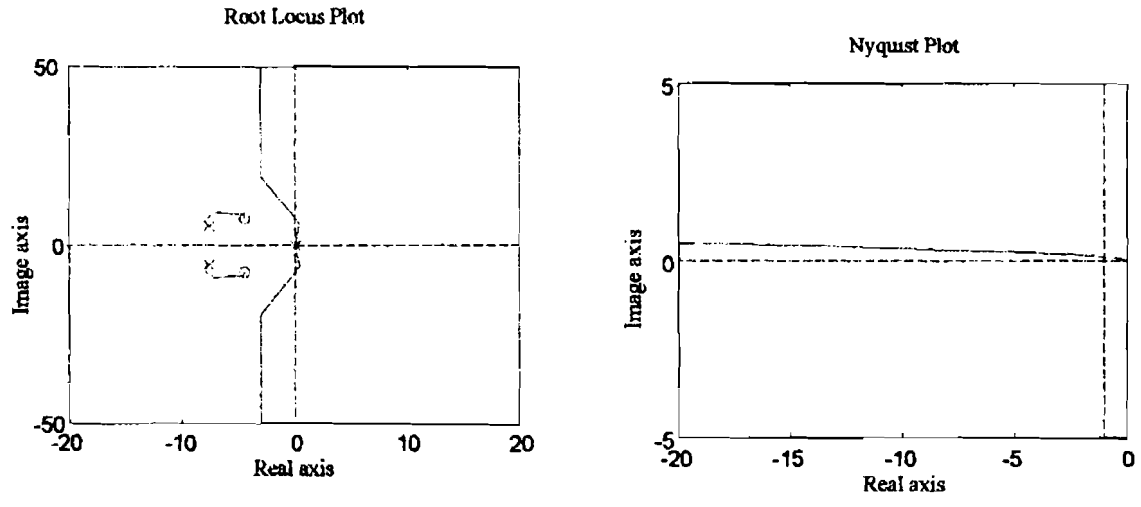

(a) (b)

Fig. 6. Stability analysis for $\ell = 2$m, $U = 30$m/s, and $t_d = 0$ s. (a) Root locus (conditional stable) (b) Nyquist plot, for unity feedback (unstable).

With this feedback signal, the unity feedback control system with the control law (11) contains a derivative compensation term proportional to the reciprocal of the vehicle speed U. There also exists a proportional compensation term, which is proportional to the reciprocal of the look-ahead distance. Roughly speaking, the closed-loop stability can be enhanced by decreasing the vehicle speed or increasing the look-ahead distance.

Now consider the closed-loop dynamics from the curvature input to the vision output. Hereafter, it will be called the disturbance response. Under the assumption of zero sensor noise, the vision output can be calculated from the block diagram (Figure 3) and the vehicle dynamics of Equation (8) as

$$\begin{aligned} y(s) &= \frac{f}{\ell}(Y_c(s) + Y_v(s)) \\ &= \frac{f}{\ell}\left(\frac{\ell^2}{2}e^{\frac{\ell}{2U}s}\rho(s)\right. \\ &\quad \left. +(-P_1(s) - \ell P_3(s))\delta(s) + (-P_2(s) - \ell P_4(s))\rho(s)\right) \\ &= -\frac{f}{\ell}(P_1(s) + \ell P_3(s))C(s)e^{-t_d s}y(s) \\ &\quad + \left\{\frac{f\ell}{2}e^{\frac{\ell}{2U}s} - \frac{f}{\ell}(P_2(s) + \ell P_4(s))\right\}\rho(s) \end{aligned} \tag{13}$$

Therefore the disturbance response is written as,

$$\frac{y(s)}{\rho(s)} = \frac{\frac{f\ell}{2}e^{\frac{\ell}{2U}s} - \frac{f}{\ell}(P_2(s) + \ell P_4(s))}{1 + \frac{f}{\ell}(P_1(s) + \ell P_3(s))C(s)e^{-t_d s}} \tag{14}$$

Table 1. Simulation parameters.

Parameter	Value
Vehicle mass, m	1573 Kg
Vehicular yaw inertia, I_z	2872 Kg-m^2
Distance from c.g to front axle, a	1.034 m
Distance from c.g to rear axle, b	1.491 m
Cornering stiffness of front wheel, C_f	95316 Nt/rad
Cornering stiffness of front wheel, C_r	95316 Nt/rad
Focal length, f	0.028 m
Pixel interval length, c	0.000004 m

The characteristic equation (CE) for the closed-loop system is

$$1 + \frac{f}{\ell}(P_1(s) + \ell P_3(s))C(s)e^{-t_d s} \triangleq 1 + L_p(s) = 0 \tag{15}$$

where L_p(s) is the loop-transfer function which determines the stability of the closed-loop system. The frequency response of $L_p(s)$ and roots of CE will be examined for a range of parameters.

We summarize below results of a numerical study conducted for the vehicle parameters in Table 1.

4.2.1. Effect of look-ahead distance on the feedback loop without time delay

The larger look-ahead distance ℓ makes the system more stable. The change of ℓ dose not affect the pole locations of $L_p(s)$ but the zero locations. By comparing Figures 4, 5 and 6, it can be observed that two zeros are on the negative real axis when ℓ is large. One of these zeros approaches the origin when ℓ is sufficiently large, and it cancels one of the open-loop pole of $L_p(s)$ as shown in Figure 4. This pole-zero cancellation reduces the order of the system, and the system performs an "angular tracking control". It means that the heading angle is controlled to track the road direction according to Equations (6) and (12). When ℓ is smaller than a certain value, the system becomes unstable for a range of the control gain as shown in Figure 6. It should be noted that all the plots in Figure 4 to Figure 6 are obtained by purely proportional control and all the Nyquist plots are for $K_p = 1$ (unity feedback control). This analysis shows that a larger look ahead distance enhances the system stability.

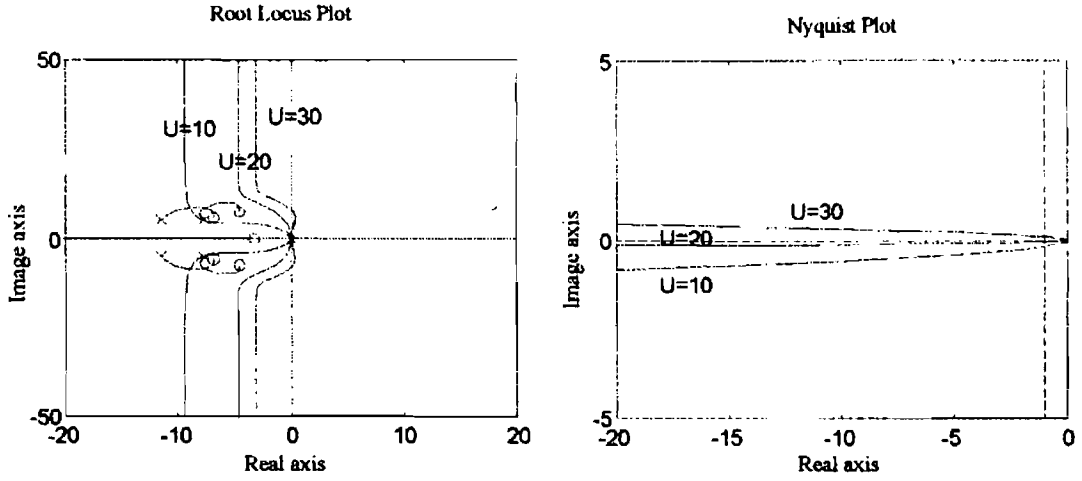

Fig. 7. Stability analysis for various longitudinal velocities, $\ell = 2$ m, $t_d = 0$ s. (a) Root locus (b) Nyquist plot, for unity feedback (unstable at $U = 30$ m/S).

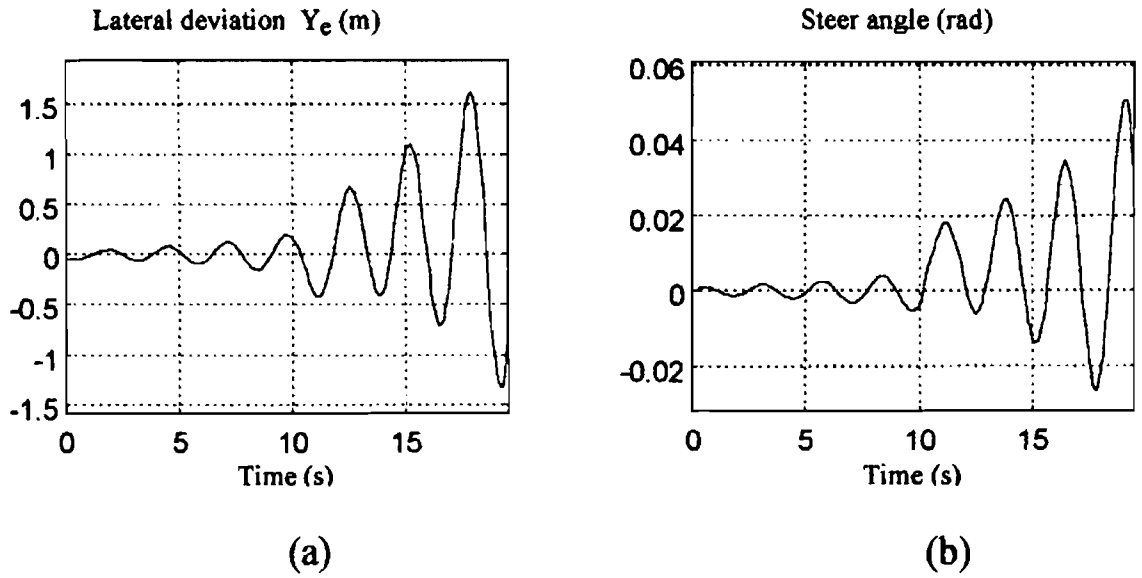

Fig. 8. Results with time delay for $\ell = 20$ m. (a) Lateral deviation (b) Steer angle.

4.2.2. Effect of vehicle speed on the feedback loop without time delay

Longitudinal velocity affects the locations of both the poles and the zeros of the loop-transfer function $L_p(s)$. The increase in the vehicle velocity shifts the root locus plot toward the right-half plane (RHP). This means that the control system is less stable at higher vehicle speeds. The system becomes conditional stable and the instability may occur for a certain range of K_p when the velocity is large. For example, the system at 30 m/s goes to instability for a range of K_p (Figure 7).

4.2.3. Effect of time delay

Time delays may result from the sampling and A/D conversion involved in the vision system as well as the processing of images and the computation of control

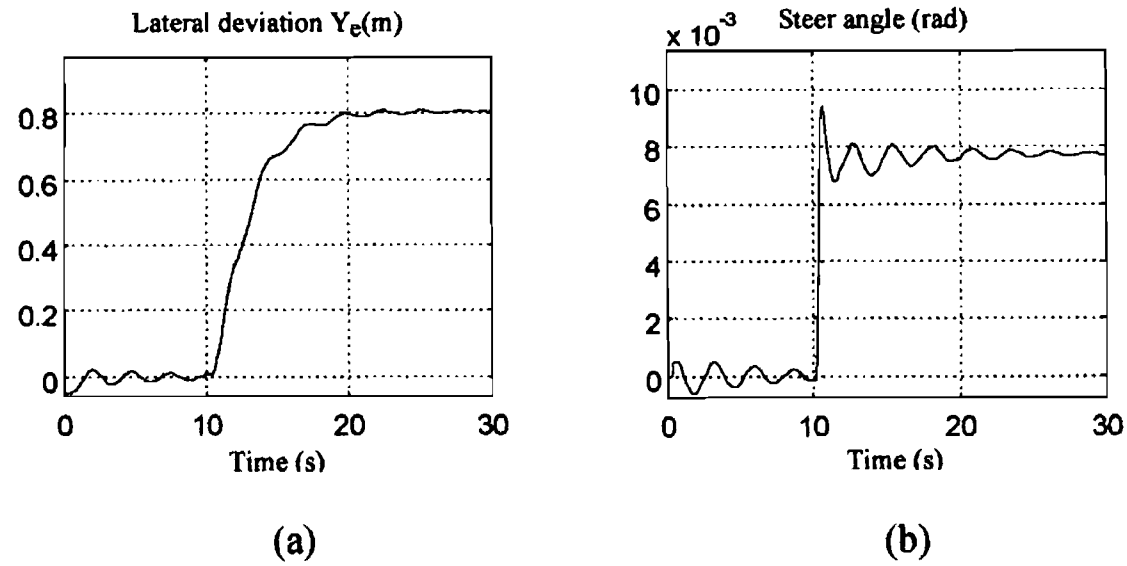

Fig. 9. Results with time delay for $\ell = 30$ m. (a) Lateral deviation (b) Steer angle.

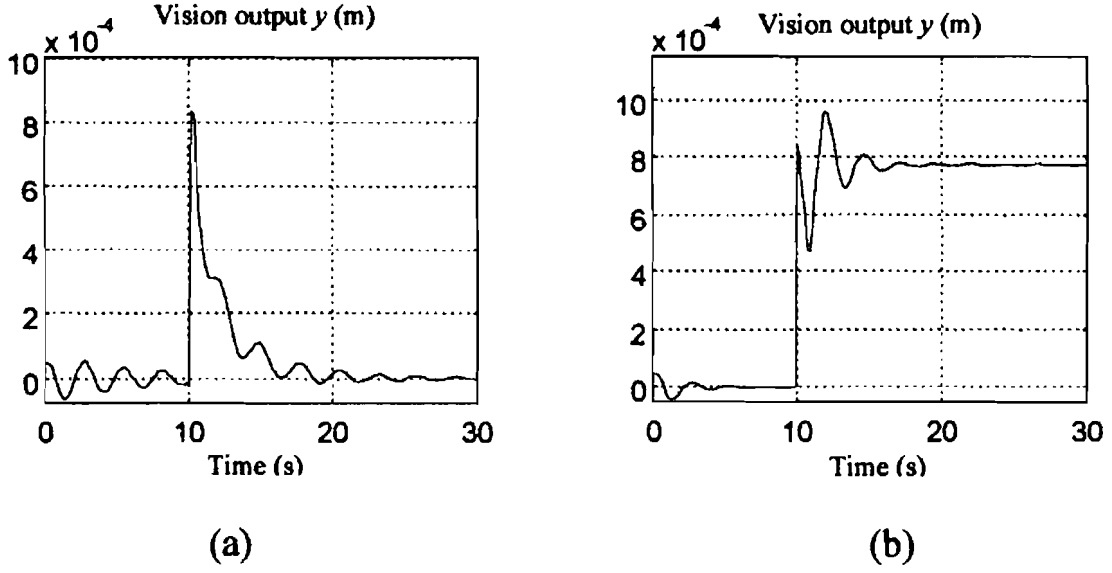

Fig. 10. Results of vision output with time delay for $\ell = 30$ m. (a) With integral control, $K_i = 5$ (b) Without integral control, $K_i = 0$.

algorithms. It may cause instability or oscillation of the feedback control system. However, this problem can be eliminated by increasing the look-ahead distance. To understand the effect of time delays, a simulation example is examined. Conditions are set as follows: the longitudinal speed U is 30 m/s, the initial lateral deviation is -0.05 m, and the curvature is initially zero and makes a step change of 0.002 1/m at 10 sec. The total time delay is 0.3 sec. The control gains of the PI controller are: $K_p = 10$, $K_i = 0$ and 5. It is assumed that there is no quantization error in the vision output.

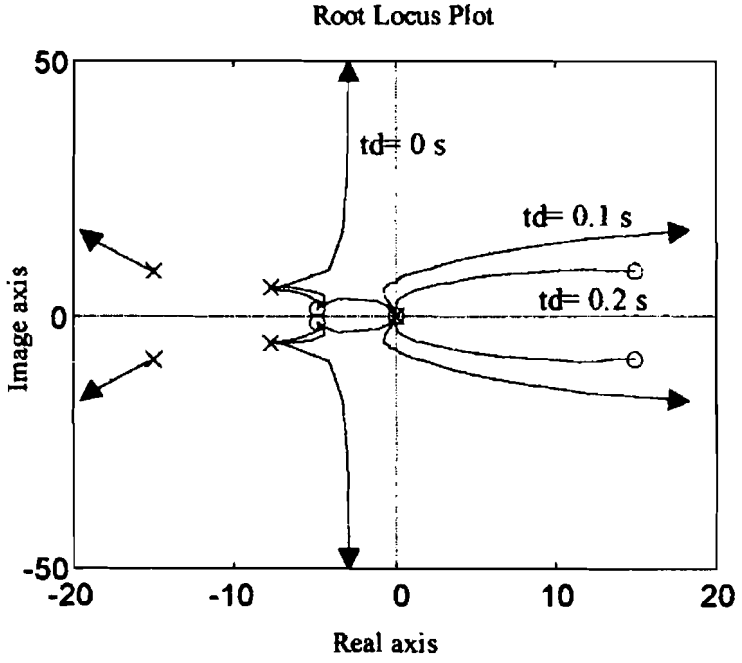

Fig. 11. Root locus plot by the effect of time delay. (U = 30 m/s, $\ell = 10$ m).

Figures 8 and 9 show the simulation results for two look-ahead distances, $\ell = 20$ m and $\ell = 30$ m, respectively, and K_I is zero. As shown in Figure 5, the system should be stable for $\ell = 20$ m if there is no time delay. Thus, the instability in Figure 8 is due to the time delay. By increasing the look-ahead distance to 30 m (Figure 9), the system is stable under the same conditions. Figure 10 shows the effect of the integral action for $\ell = 30$ m. It is observed that the vision output is regulated to zero by adding the integral control. It should be noted, however, that the actual lateral deviation dose not necessarily go to zero; in the case of Figure 10(a), the steady state lateral deviation is about 0.8 m. We will discuss the steady state error in more details later.

In Figure 11, the root loci with various delay times are shown. They are obtained by applying the 3rd order Pade approximation to the time delay, which introduces RHP zeros in the loop-transfer function $L_p(s)$. These extra RHP zeros are closer to the origin for longer delay times, and are farther away from the origin for shorter delay times. RHP zeros closer to the origin generate stronger attractions to move root loci of CE toward RHP and can deteriorate the closed-loop stability more seriously.

4.2.4. Frequency domain stability analysis

The root locus analysis relied on a Pade approximation. In order to better understand the limitations of the control system, the frequency-domain analysis is performed by varying key parameters. The Bode plot of the loop-transfer function $L_p(s)$ with the unity feedback controller is shown in Figure 12. It is observed that the phase margin increases as the look-ahead distance increases, but the cross-over

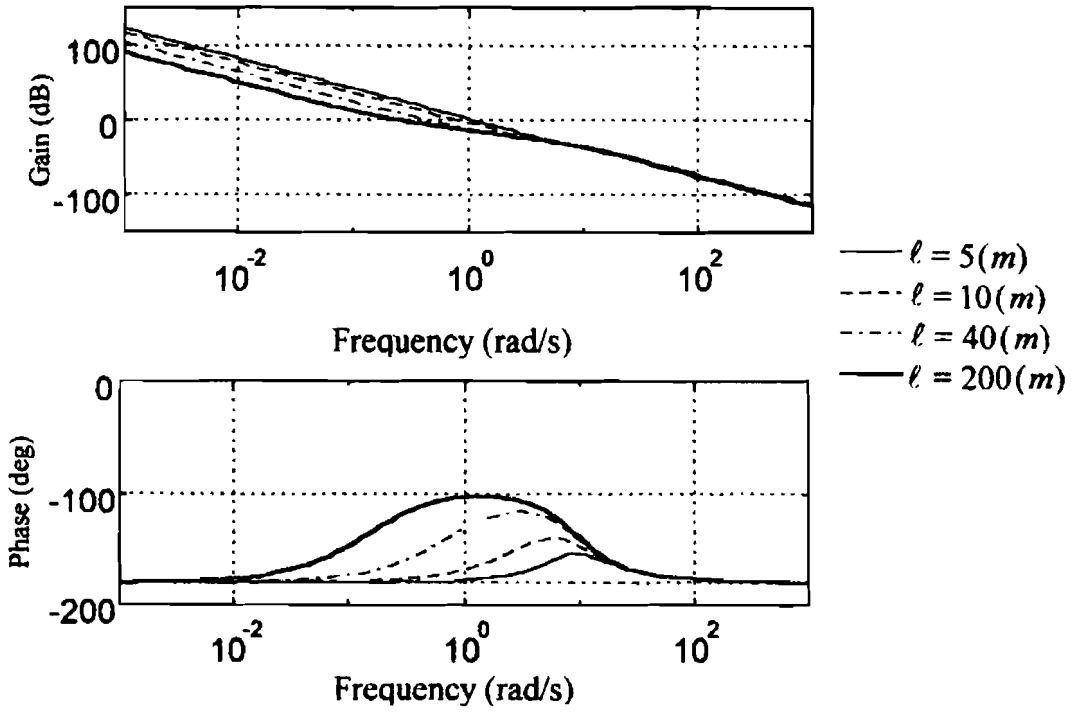

Fig. 12. Bode plot of the loop-transfer function with various look-ahead distances. ($t_d = 0$ s, unity feedback control).

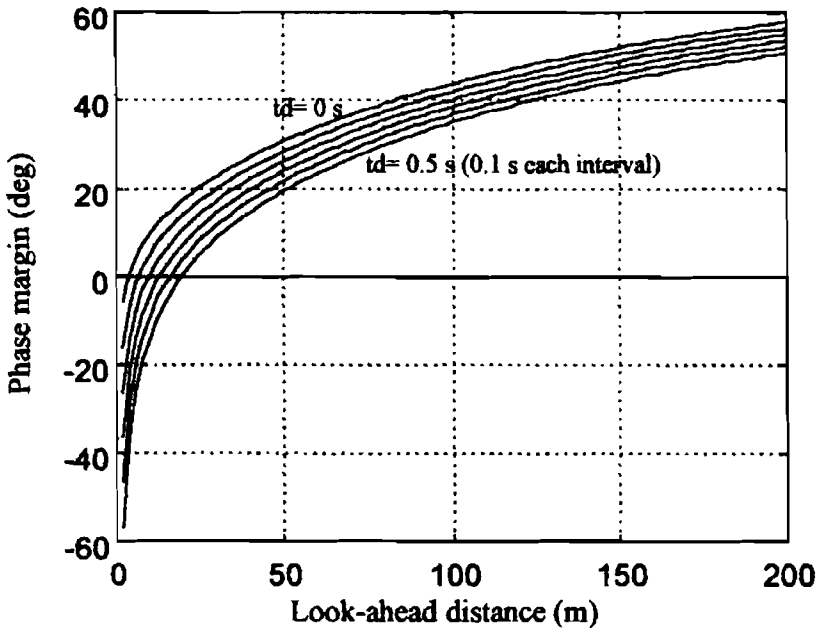

Fig. 13. Phase margin vs. look-ahead distance for selected values of delay time. ($U = 30$ m/s, unity feedback control).

frequency decreases. When the look-ahead distance is very large ($\ell = 200$ m), the system performs like a reduced-ordered system (from 2nd to 1st order) around the cross-over frequency because of the "angular tacking behavior" explained previously.

Figures 13 to 15 show the plots summarized from frequency responses for various combinations of look-ahead distance, longitudinal velocity, and delay

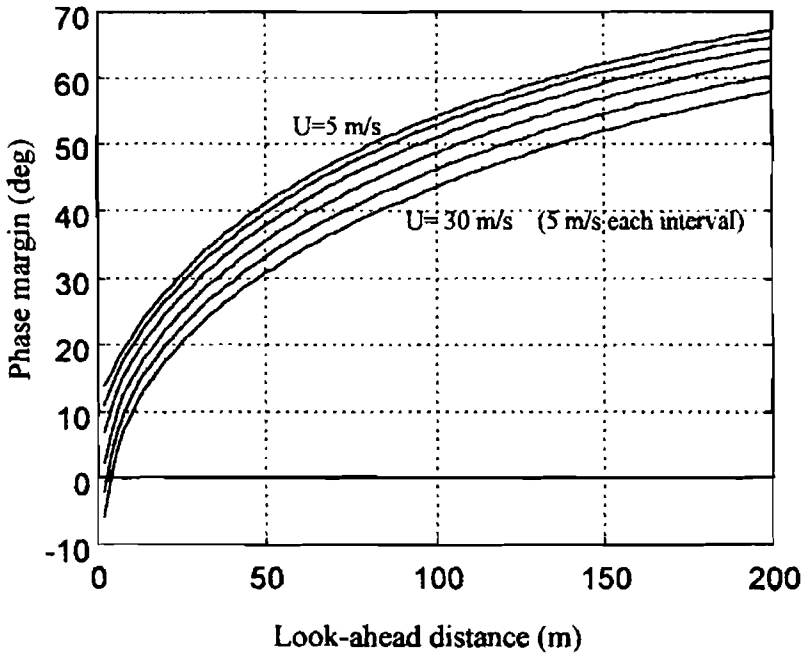

Fig. 14. Phase margin vs. look-ahead distance for selected values of vehicle speed. ($t_d = 0$ s, unity feedback).

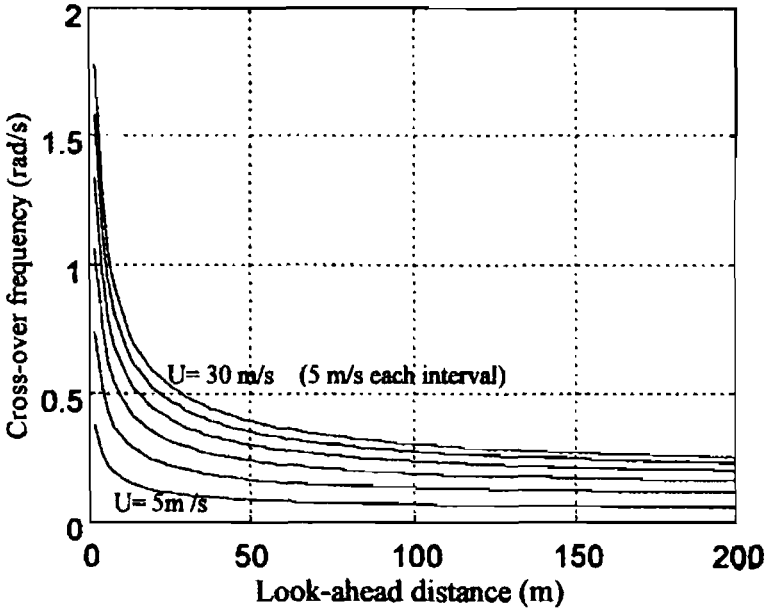

Fig. 15. Cross-over frequency vs. look-ahead distance for selected values of vehicle speed. (unity feedback control).

time. $C(s) = 1$ has been assumed. Figure 13 shows the effect of the time delay on the relationship between the phase margin and the look ahead distance for the longitudinal velocity of 30 m/s. As shown in this figure, the phase margin gradually increases to about 50 deg as the look-ahead distance extends to 200 m. The shortest admissible look-ahead distance for a stable control system is about 5 m when $t_d = 0$ s. This value should be increased to about 20 m for $t_d = 0.5$ s. The effect of the time delay on the phase margin is less significant when a larger look-ahead distance is adopted.

Figure 14 shows the effect of the speed on the relationship between the phase margin and the look ahead distance for $t_d = 0$. The unity feedback control has been assumed. Notice that the phase margin becomes smaller as the longitudinal velocity is increased.

Figure 15 shows the dependence of the gain cross-over frequency, ω_c, on the look-ahead distance for selected values of vehicle speed. The figure shows that ω_c decreases from 1.75 rad/s to 0.25 rad/s as the look-ahead distance changes from 0 to 200 m at the longitudinal velocity of 30 m/s. When the velocity is reduced, the cross-over frequency decreases.

4.3. Closed-loop Performance Analysis

4.3.1. Disturbance response

The disturbance response of the closed-loop system is characterized by the transfer function from the curvature input to the vision output as expressed by Equation (14). Its closed-loop frequency response with the unity feedback control (sensitivity function) is shown in Figure 16. To obtain zero steady-state vision outputs for

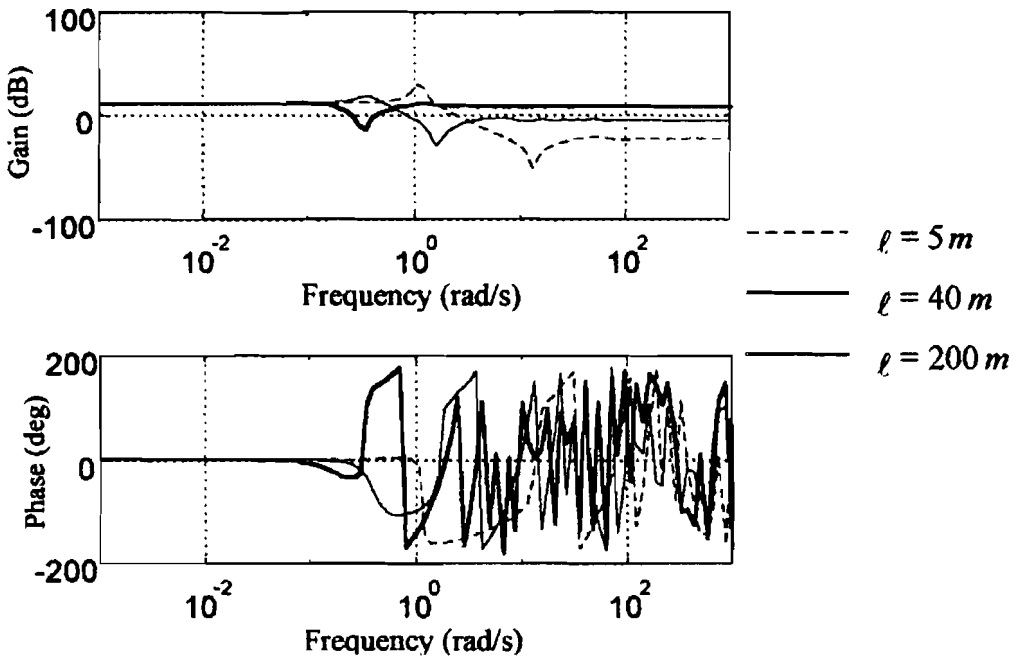

Fig. 16. Bode plot of the disturbance response without integral control. ($K_p = 1$, $K_i = 0$, $U = 30$ m/s, $t_d = 0$ s).

constant curvature inputs, an integral control action can be added (Figure 17). The fundamental difference between these two cases is that the closed-loop gain is reduced at low frequencies by the integral control. The common characteristics

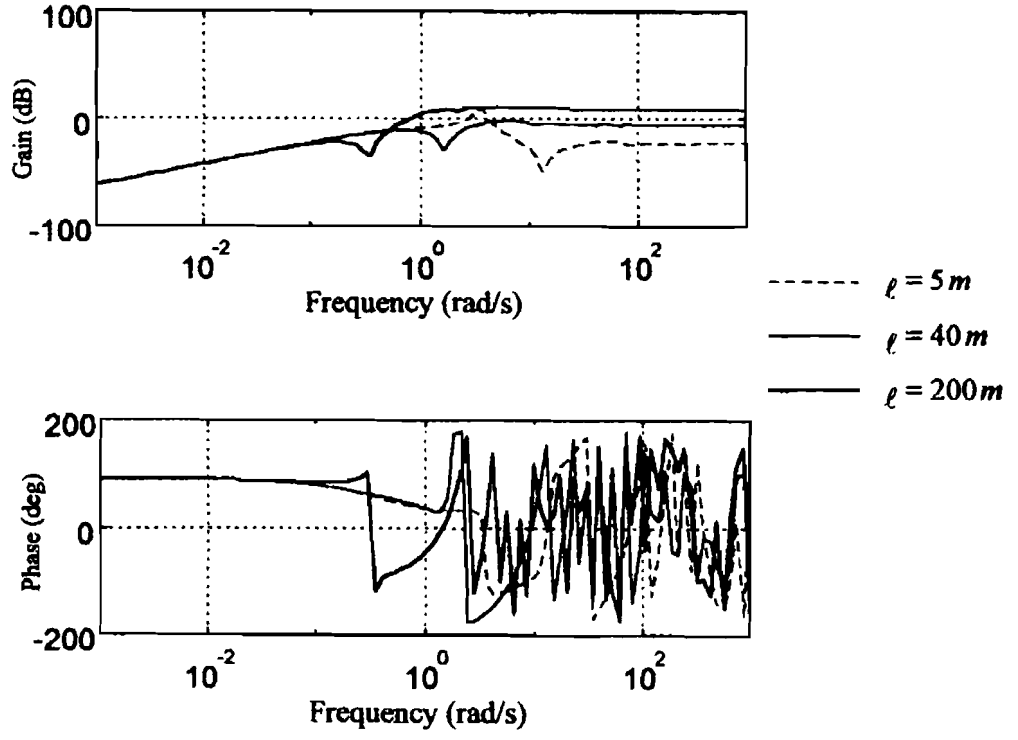

Fig. 17. Bode plot of the disturbance response with integral control. ($K_p = 10$, $K_i = 5$, $U = 30$ m/s, $t_d = 0$ s).

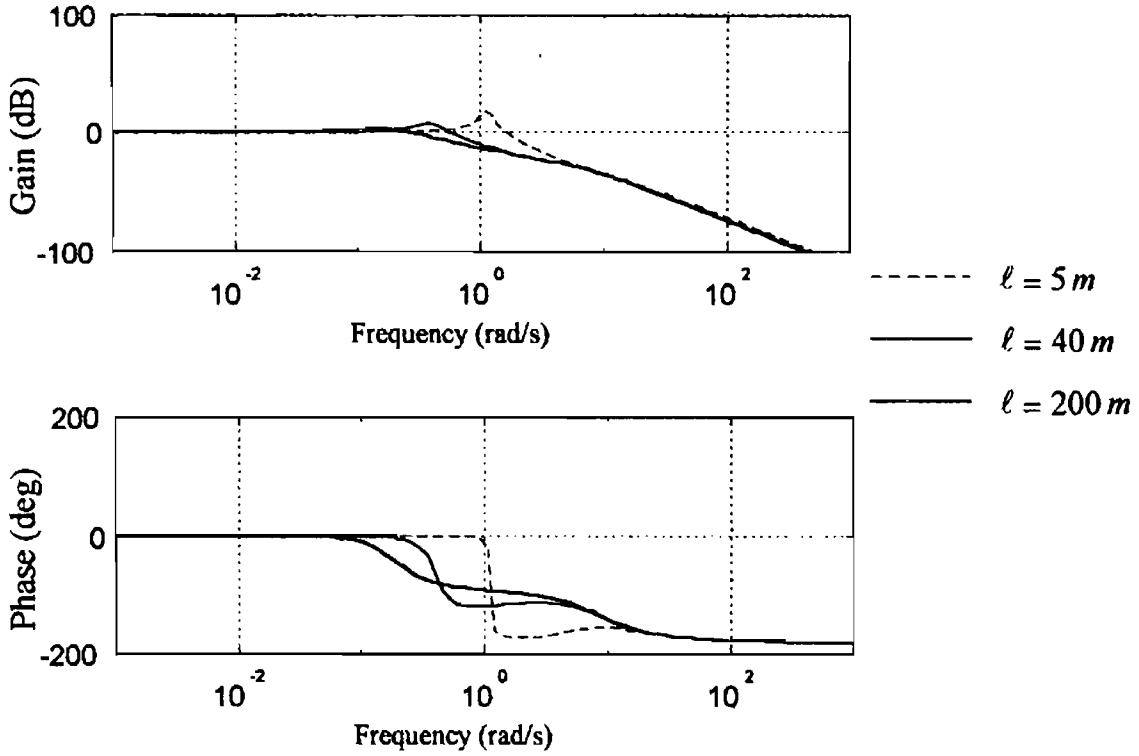

Fig. 18. Bode plot of the tracking response. ($K_p = 1$, $K_i = 0$, $U = 30$ m/s, $t_d = 0$ s).

between the two are: (1) there is a notch-filter-like behavior around 10 rad/s and (2) the longer the look-ahead distance, the lower the frequency of the notch. In the low frequency range, the gain does not depend on the look-ahead distance. However, the gain is smaller for shorter look-ahead distances at high frequencies. It means that the closer vision information is required when the vehicle must track the road with high frequency contents.

4.3.2. Tracking response

The tracking response of the closed-loop system is defined by the transfer function from the road position Y_c to $-Y_v$. From Figure 3, the tracking response can be written as

$$\frac{-Y_v(s)}{Y_c(s)} = \frac{\frac{f}{\ell}(P_1(s) + \ell P_3(s))C(s)e^{-t_d s}}{1 + \frac{f}{\ell}(P_1(s) + \ell P_3(s))C(s)e^{-t_d s}} = \frac{L_p(s)}{1 + L_p(s)} \tag{16}$$

which is the complementary sensitivity function. The frequency response plot of (16) for the unity feedback control system is shown in Figure 18. It is observed that the longer the look-ahead distance, the smaller the tracking bandwidth. This tracking control system behaves like a low-pass filer for the road path. A longer look-ahead distance implies a smaller cut-off frequency, which is suitable for smooth roads. If the road profile includes high frequency contents, a shorter look-ahead distance is required.

4.4.3. Steady state error analysis

The actual lateral deviation Y_e at c.g., rather than the vision output y, is usually the major concern of the lateral control system. Under a given constant road curvature, the related state vector and the control action at the steady state can be obtained by setting $\frac{\mathrm{d}\boldsymbol{x}}{\mathrm{d}t} = 0$ in Equation (1): i.e.,

$$\dot{\boldsymbol{x}} = 0$$

$$\Rightarrow$$

$$r_{ss} = U\rho$$

$$\beta_{ss} = \frac{-aC_f mU^2 + 2b(a+b)C_f C_r}{2(a+b)C_f C_r}\rho = G_\beta \rho$$

$$\varphi_{h\_ss} = -\beta_{ss} = -G_\beta \rho$$

$$\delta_{ss} = \frac{(-aC_f + bC_r)mU^2 + 2(a+b)^2 C_f C_r}{2(a+b)C_f C_r} = \rho = G_\delta \rho \tag{17}$$

The steady-state value of lateral deviation at c.g., i.e., Y_{e_ss} can not be determined by the vehicle dynamic equation. It depends on the control law used for closed-loop control.

For the unity feedback control law,

$$\delta_{ss} = \frac{f}{\ell} Y_{v\_ss} + \frac{f}{\ell} Y_{c\_ss}$$

$$= -\frac{f}{\ell}\left(Y_{e\_ss} + \ell\varphi_{h\_ss}\right) + \frac{f\ell}{2}\rho$$

$$\Rightarrow$$

$$Y_{e\_ss} = -\frac{\ell}{f}\delta_{ss} - \ell\varphi_{h\_ss} + \frac{\ell^2}{2}\rho$$

$$= \left(-\frac{G_\delta}{f} + G_\beta + \frac{\ell}{2}\right)\ell\rho \tag{18}$$

For the integral control on the vision output,

$$y_{ss} = \frac{f}{\ell}(Y_{v\_ss} + Y_{c\_ss})$$

$$= \frac{f}{\ell}\left(-Y_{e\_ss} - \ell\varphi_{h\_ss} + \frac{\ell^2}{2}\rho\right)$$

$$= 0$$

$$\Rightarrow$$

$$Y_{e\_ss} = -\ell\varphi_{h\_ss} + \frac{\ell^2}{2}\rho$$

$$= \left(G_\beta + \frac{\ell}{2}\right)\ell\rho \tag{19}$$

From (18) and (19), the steady-state lateral deviation is proportional to the curvature disturbance and increases as the look-ahead distance is increased for both the unity feedback control and the integral control.

4.4.4. Sensitivity to sensor noise

The sensitivity of the vision output with respect to the sensor noise can be derived from Figure 3 as

$$\frac{y(s)}{n(s)} = \frac{-\frac{f}{\ell}(P_1(s) + \ell P_3(s))C(s)e^{-t_d s}}{1 + \frac{f}{\ell}(P_1(s) + \ell P_3(s))C(s)e^{-t_d s}} = \frac{-L_p(s)}{1 + L_p(s)} \tag{20}$$

The frequency response gain of this transfer function is the same as that of Equation (16). From Figure 18, it can be concluded that the noise attenuation is better in the frequency range around ω_c if a longer look-head distance is used.

5. VISION-BASED LATERAL CONTROLLER DESIGN

In this section, we discuss the redesign of the control system in Figure 3 for a better performance. The necessity for estimating the vehicle state variables and the curvature is found from the analysis in the previous section. In particular, we note that the actual lateral deviation at c.g. is not directly available from the vision output and that the selection of look-ahead distances must take into consideration the vision delay. A new control system architecture is proposed in Figure 19. It

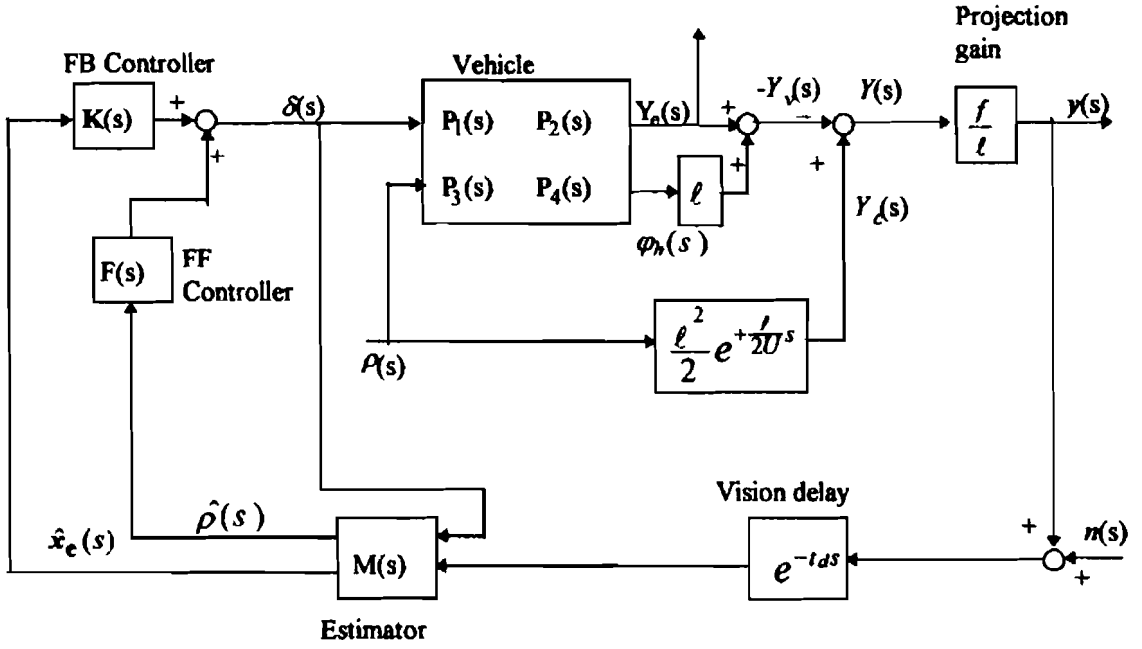

Fig. 19. Block diagram for the new control system with estimator and FF controller.

differs from the controller considered in the previous section in several regards. It has an estimator for the curvature and the error vector x_e from the vision outputs. The error vector is the difference between the actual state vector and the desired and contains the steady state values in (17). The desired Y_e is set to zero.

5.1. Feedforward (FF) Controller

The purpose of the FF controller is to let the vehicle track the road of any curvature. In the lateral control systems without vision, the disturbance (road curvature) is not directly measured. However, in the vision-based system, the road curvature ahead of the vehicle can be previewed and its effect may be eliminated by using a suitable FF controller.

According to Equation (8), the lateral deviation caused by the curvature ρ is $P_2(s)\rho$. This should be canceled out by the steering input: i.e. the input channel should subtract $P_1^{-1}(s)P_2(s)\rho$ to eliminate the curvature effect. Therefore, the proposed FF controller is

$$F(s) = -P_1^{-1}(s)P_2(s) \tag{21}$$

This FF controller ensures perfect tracking of the road. For this FF controller to work $P_1(s)$, should not possess unstable zeros.

In the presence of vision delays, the curvature ahead of the vehicle should be estimated and used as the input to the FF controller. In this case, the estimated curvature obtained after a time delay t_d, is give by

$$\hat{\rho}(s) = \rho(s)e^{-t_d s}$$

If $\hat{\rho}(s)$ is the input to the FF controller, $F(s)$ should be modified to

$$F(s) = -P_1^{-1}(s)P_2(s)e^{t_d s}$$

It means that the previewed curvature at an equivalent look ahead distance of $\ell = Ut_d$ should be used as the input to the FF controller in Equation (21).

5.2. Feedback (FB) Controller

The feedback controller determines the stability and bandwidth of the closed-loop system. For a given specification on noise sensitivity, bandwidth, stability robustness, and steady-state error, the FB controller can be designed by using several methods such as PID, LQG, FSLQ, and μ-synthesis. To stabilize the closed-loop system with the vision delay, the nominal loop-transfer function (for $t_d = 0$) should be synthesized with a sufficiently large phase margin. The time delay t_d can result in the phase lag of $\omega_c t_d$(rad) at the gain cross-over frequency ω_c(rad/s). Therefore, to avoid instability, the phase margin for the synthesized nominal loop-transfer function should be larger than $\omega_c t_d$(rad).

5.3. Estimator

The estimator is required to estimate the essential state variables of the vehicle and the previewed road curvatures. According to the measurement matrix in Equation (7), the lateral deviation Y_e and the heading angle φ_h may be extracted from the vision outputs at all scanning levels. By the least square method, the reliable estimates can be expressed as

$$\begin{bmatrix} \varphi_h(t) \\ Y_e(t) \end{bmatrix} = (\mathbf{H}_1^* \mathbf{H}_1)^{-1} \mathbf{H}_1^* y_v(t) \tag{22}$$

For the AHS application, where the road curvature is normally small, the road within a small look-ahead distance can be approximated as a straight line. Therefore, the vision outputs y in the lower portion of the image plane can be considered as y_v in Equation (22). Other state variables of the vehicle can be estimated by a Luenburger observer.

The road curvatures ahead of the vehicle may also be extracted from the vision output. From Equations (2) and (3), the curvatures corresponding to various regions of the road ahead of the vehicle satisfy

$$\rho(\ell, t) = \frac{\partial^2 Y(\ell, t)}{\partial \ell^2} = \frac{\partial^2 \left(\frac{\ell}{f} y(\ell, t) \right)}{\partial \ell^2} \tag{23}$$

The second derivative on the right-hand side may be obtained from the image. However, the direct numerical differentiation will introduce serious errors due to

noises and quantization errors. To overcome this problem, the estimation will be performed by considering the road as overlapping regions of constant curvatures. According to Equation (2) and Figure 1, the following geometric relations still hold for a region with piecewise constant curvature:

$$Y(\ell_{k+q}, t) - Y(\ell_{k-q}, t) = \varphi_r(\ell_{k-q}, t)(\ell_{k+q} - \ell_{k-q}) + \frac{\rho(\ell_k, t)}{2}(\ell_{k+q} - \ell_{k-q})^2 \tag{24a}$$

$$Y(\ell_k, t) - Y(\ell_{k-q}, t) = \varphi_r(\ell_{k-q}, t)(\ell_{k+q} - \ell_{k-q}) + \frac{\rho(\ell_k, t)}{2}(\ell_k - \ell_{k-q})^2$$

$$\text{for} \quad k = q+1, \ldots, N-q \tag{24b}$$

where $\varphi_r(\ell_{k-q}, t)$ is the relative angle between the vehicle heading and the road at the look ahead distance ℓ_{k-q} at time t. $\rho(\ell_k, t)$ is the equivalent curvature in the region from ℓ_{k-q} to ℓ_{k+q}. The number of overlaps between regions of different curvatures is $2q$. N is the number of scanning levels on the image plane. Equalities (24a) and (24b) can be used to eliminate $\varphi_r(\ell_{k-q}, t)$. The curvature in this region $\rho(\ell_k, t)$ can be calculated as

$$\rho(\ell_k, t) = \frac{2}{\ell_{k+q} - \ell_k}\left[\frac{Y(\ell_{k+q}, t) - Y(\ell_{k-q}, t)}{\ell_{k+q} - \ell_{k-q}} - \frac{Y(\ell_k, t) - Y(\ell_{k-q}, t)}{\ell_k - \ell_{k-q}}\right]$$

$$= \frac{2}{f(\ell_{k+q} - \ell_k)}\left[\frac{\ell_{k+q} y(\ell_{k+q}, t) - \ell_{k-q} y(\ell_{k-q}, t)}{\ell_{k+q} - \ell_{k-q}} - \frac{\ell_k y(\ell_k, t) - \ell_{k-q} y(\ell_{k-q}, t)}{\ell_k - \ell_{k-q}}\right]$$

$$\text{for } k = q+1, \ldots, N-q \tag{25}$$

It can be expected that larger the overlap number q, smoother the estimated curvature. However, the estimation is distorted if q is larger.

5.4. Design Example

Consider a vision-based lateral control system with parameters listed in Table 1. The vision delay is 200 ms, the previewed region is from 3 m to 40 m ahead of the vehicle, the total number of scanning levels N is 30 and the overlap number q is 3. The estimated value of the curvature is restricted below 0.004 m^{-1} in absolute value based on a prior knowledge of the configured highway. The road curvature

is 0 m^{-1} from 0 to 3 second (0 to 90 m), 0.002 m^{-1} from 3 to 6 second (90 to 180 m), and -0.001 m^{-1} from 6 to 10 second (180 to 300 m). The steering actuator is limited by a magnitude constraint, $|\delta| < \bar{\delta} = 0.5$ rad, and a rate constraint, $|\dot{\delta}| < \dot{\bar{\delta}} = 1$ rad/s. The vehicle longitudinal velocity is 30 m/s. The initial state variables of the vehicle are: $r = 0$, $\beta = 0$, $\varphi_h = 0$, $Y_e = -0.05$ m.

The FF controller in Equation (21) is used with previewed curvature at a look-ahead distance of 6 m, which corresponds to a look-ahead time of 0.2 sec at the assumed velocity. The PID law is applied to the FB controller with the feedback of extracted Y_e from the vision outputs. From Figure 19, the loop-transfer function for this design is: $L_p(s) = P_1(s)C(s)e^{-t_d s}$, where $C(s)$ is the PID controller as defined by Equation (10). Parameters of the controller are chosen as: $K_p = -0.01$, $K_i = 0$, $K_d = -0.0074$ and $T_i = 0.0001$. In this combination, the loop-transfer function of the system has the cross-over frequency, 2 rad/s, and the phase margin, 41.54 deg, for the nominal case ($t_d = 0$). Note that this is greater than 2 (rad/s)* 0.2 (rad)* 180/Pi (deg/rad) = 22.95 deg, the value required to stabilize the feedback system with the assumed vision delay time.

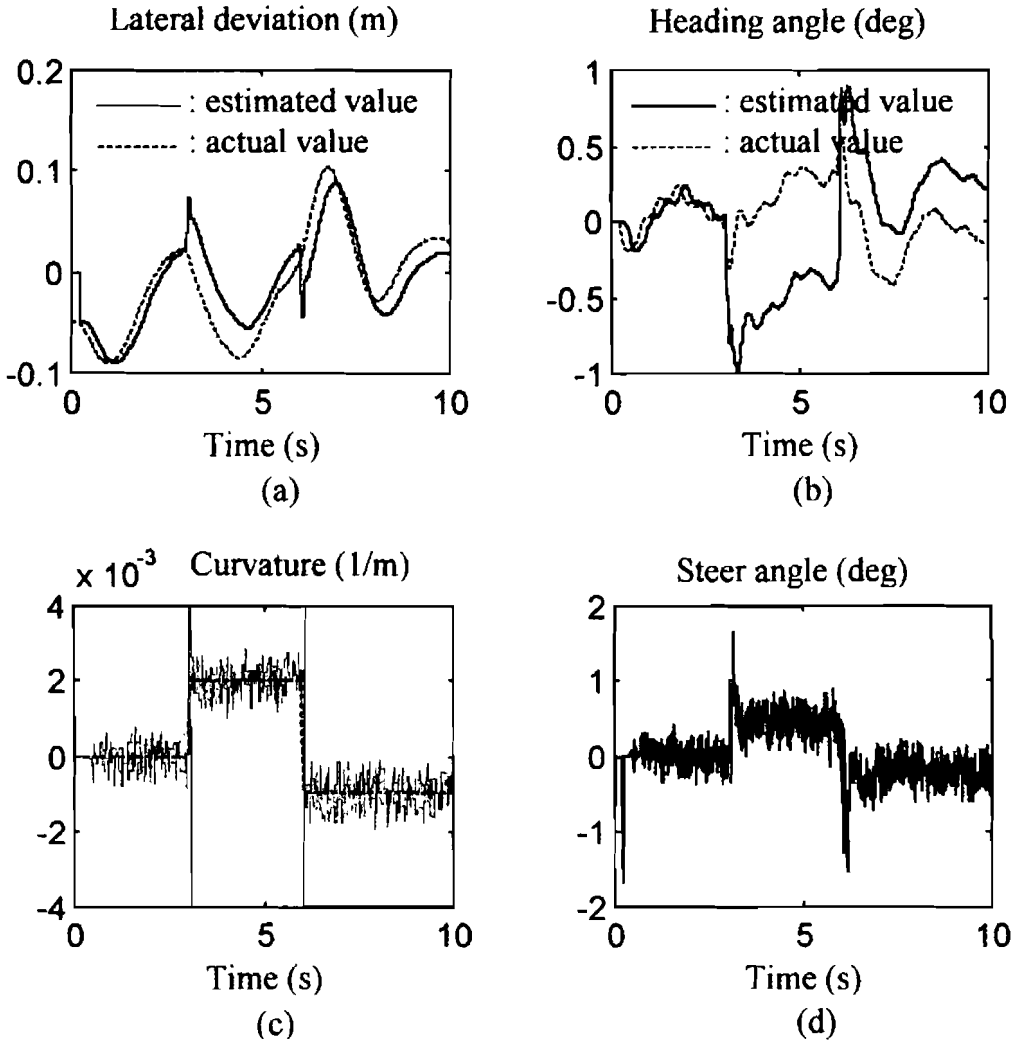

Fig. 20. Results of the new control system with estimator and FF controller. (a) Lateral deviation (b) Heading angle (c) Road curvature (d) Steer angle.

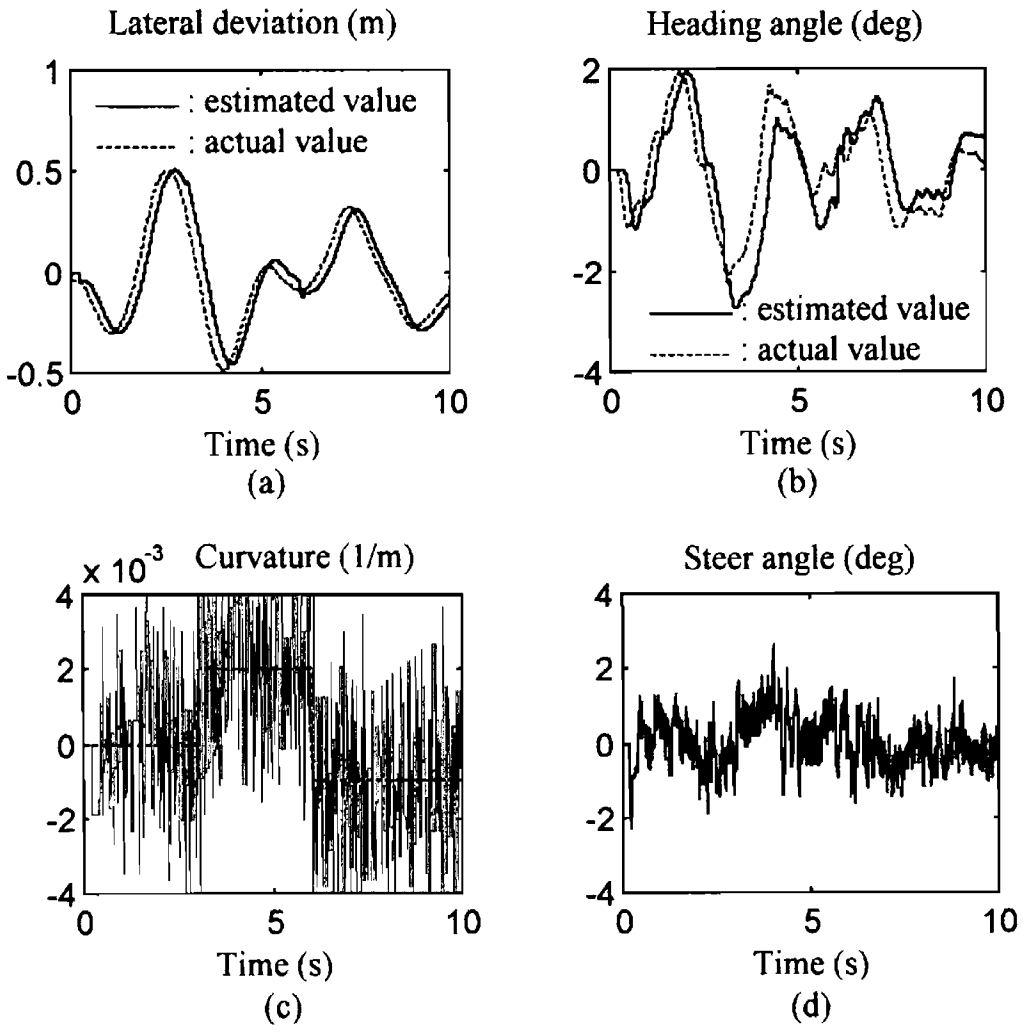

Fig. 21. Results of the new control system with lower resolution camera. (a) Lateral deviation (b) Heading angle (c) Road curvature (d) Steer angle.

The time histories of the lateral deviation, heading angle, estimated curvature at the specified look-ahead distance and steer angle for this example are shown in Figures 20(a) to (d). The estimate of the road curvature remains close to the actual curvature. On the other hand, the estimation scheme (22) for the lateral deviation and heading angle introduces offset errors at instances when the road curvature is not zero. These offset errors are caused by considering the curved road at the lower portion of the image as a straight road. The vehicle can track the road stably with small lateral deviations. The error in the curvature estimation could be the reason that the lateral deviation is not zero during the transition of the curvature change. On the other hand, if the resolution of the camera is deteriorated by increasing the size of pixel five times the nominal one, the results are as shown in Figure 21(a) to (d). The estimates from the vision signal are significantly degraded, and the control performance is deteriorated. This shows that the sensor noise and the quantization error can affect the control performance significantly in the vision-based lateral control system.

6. CONCLUSIONS

Vision based lateral control systems have been proposed in various forms including the early work by Dickmanns and co-workers [2,3] and several systems presented at the Demonstration '97 in San Diego by National Automated Highway Systems Consortium. Despite of these successful implementation examples, vision-based lateral control has not been fully studied by analysis. In this paper, the effect of various factors in the vision-based lateral control system with the direct feedback of the vision output have been analyzed. They are summarized as follows:

(1) Look-ahead distance:

Increasing the look-ahead distance enhances the stability but increases the error and decreases the closed-loop bandwidth. A longer look-ahead distance results in the closed-loop behavior similar to the angular tracking control or the derivative compensation. The upper bound of the look-ahead distance is limited by the quantization error of the image and the specification of control performance. The lower bound is determined by the system stability requirement.

(2) Time delay in the feedback path:

Introduction of the time delay will cause instability, including the reduction of the phase margin and the equivalent effect of RHP zeros appearing in the loop-transfer function.

(3) Vehicle speed:

A higher vehicle speed will increase the cross-over frequency but may cause instability.

(4) Control system design and challenges:

The state estimation is required to obtain accurate curvature and lateral deviation for better control. A feasible solution to extract those variables has been suggested, and a FF controller for perfect tracking has been proposed. A design example with time delay using simple PID control has also been illustrated. The performance is seriously degraded by the sensor noise which includes the quantization error of the image.

ACKNOWLEDGEMENT

This work was in part supported by the California PATH (Partners for Advanced Transit and Highways) Research Program.

REFERENCES

[1] Masaki, I. (Ed.): Vision-based Vehicle Guidance, Springer-Verlag, 1992.

[2] Dickmanns, E.D., and Graefe, V.: Applications of dynamic monocular machine vision. Machine Vision Applications 1 (1988), pp. 241–261.

[3] Dickmanns, E.D. and Mysliwetz, B.D.: Recursive 3-D road and relative ego-state recognition. IEEE Transaction on Pattern Analysis and Machine Intelligence 4 (1992), pp. 199–213.
[4] Peng, H. and Tomizuka, M.: Preview control for vehicle lateral guidance in highway automation. ASME Journal of Dynamic Systems, Measurement, and Control 115 (1993), pp. 679–686.
[5] Lee, A.Y.: A preview steering autopilot control algorithm for four-wheel-steering passenger vehicles. ASME Journal of Dynamic Systems, Measurement, and Control 114 (1992), pp. 401–408.
[6] Guldner, J., Tan, H.-S. and Patwardhan, S.: Analysis of automatic steering control for highway vehicles with look-down lateral reference systems. PATH Technical Note 96-3, Institution of Transportation Studies, University of California, Berkeley, 1996.
[7] Shladover, S.E., Wormley, D.N., Richardson, H.H. and Fish, R.: Steering controller design for automated guideway transit vehicles. ASME Journal of Dynamic Systems, Measurement, and Control 100 (1978), pp. 1–8.